*Cerebral Cortex*, February 2016;26: 683–694

**doi: 10.1093/cercor/bhu248**
Advance Access Publication Date: 20 October 2014
ORIGINAL ARTICLE

ORIGINAL ARTICLE

# Low- but Not High-Frequency LFP Correlates with Spontaneous BOLD Fluctuations in Rat Whisker Barrel Cortex

Hanbing Lu[1], Leiming Wang[1], William W. Rea[1,2], Julia K. Brynildsen[1], Saul Jaime[1,3], Yantao Zuo[1,4], Elliot A. Stein[1], and Yihong Yang[1]

[1]Neuroimaging Research Branch and [2]Integrative Neurobiology Section, National Institute on Drug Abuse, Intramural Research Program, National Institutes of Health, Baltimore, MD 21224, USA, [3]Department of Physiology, School of Medicine, University of Texas Health Science Center in San Antonio, TX 78229, USA and [4]Psychiatry and Behavioral Sciences, Duke University School of Medicine, Durham, NC 27705, USA

Address correspondence to Dr Hanbing Lu, 251 Bayview Boulevard, Suite 200, Rm 07A727, Baltimore, MD 21224, USA. Email: luha@intra.nida.nih.gov

## Abstract

Resting-state magnetic resonance imaging (rsMRI) is thought to reflect ongoing spontaneous brain activity. However, the precise neurophysiological basis of rsMRI signal remains elusive. Converging evidence supports the notion that local field potential (LFP) signal in the high-frequency range correlates with fMRI response evoked by a task (e.g., visual stimulation). It remains uncertain whether this relationship extends to rsMRI. In this study, we systematically modulated LFP signal in the whisker barrel cortex (WBC) by unilateral deflection of rat whiskers. Results show that functional connectivity between bilateral WBC was significantly modulated at the 2 Hz, but not at the 4 or 6 Hz, stimulus condition. Electrophysiologically, only in the low-frequency range (<5 Hz) was the LFP power synchrony in bilateral WBC significantly modulated at 2 Hz, but not at 4- or 6-Hz whisker stimulation, thus distinguishing these 2 experimental conditions, and paralleling the findings in rsMRI. LFP power synchrony in other frequency ranges was modulated in a way that was neither unique to the specific stimulus conditions nor parallel to the fMRI results. Our results support the hypothesis that emphasizes the role of low-frequency LFP signal underlying rsMRI.

**Key words:** barrel cortex, gamma oscillation, delta oscillation, spontaneous fluctuation, functional connectivity

## Introduction

Spontaneous intrinsic neuronal activity is a prominent feature of the mammalian brain (Buzsaki and Draguhn 2004). Seemingly random noise in the resting-state magnetic resonance imaging (rsMRI) signal has been exploited to identify a number of "resting-state brain networks" (Biswal et al. 1995; Raichle 2011). Alterations in such network activity are implicated in a range of neurodegenerative and neuropsychological diseases, including Alzheimer's disease (Li et al. 2002; Lustig et al. 2003; Greicius et al. 2004), depression (Anand et al. 2003; Greicius et al. 2007), and drug addiction (Hong et al. 2009; Gu et al. 2010; Tomasi et al. 2010). Despite clinical potential of this technique (Greicius 2008), the underlying mechanism and physiological relevance of the fluctuations remain poorly understood (Leopold and Maier 2012).

Several lines of evidence suggest the important role of spontaneous slow and infraslow electroencephalographic (EEG) oscillations underlying the low-frequency blood oxygenation level–dependent (BOLD) fluctuations (Lu et al. 2007; He et al. 2008; Pan et al. 2013). However, contrasting hypotheses emphasize the role of higher frequency (gamma) EEG activity in the

BOLD fluctuations (Nir et al. 2008; Shmuel and Leopold 2008; Schölvinck et al. 2010). Mounting evidence supports the proposition that gamma enhancement reflects a state of high neuronal excitability and synchrony, and is involved in a number of brain operations, ranging from sensory perception, to perceptual binding, selective attention and memory (Engel et al. 1999; Fries et al. 2007; Jensen et al. 2007; Schroeder and Lakatos 2012). However, the amplitude of gamma activity is often coupled with the phase of lower frequency delta and theta oscillations (Chrobak and Buzsaki 1998; Buzsaki et al. 2003; Lakatos et al. 2005).

One approach to disentangle the relationship between electrophysiological and rsMRI signals is to investigate how an evoked response interacts with ongoing spontaneous brain activity. Previous electrophysiological (Arieli et al. 1995, 1996) and functional MRI studies (Fox et al. 2006) suggested an approximately linear superposition between the evoked and the ongoing spontaneous activity, implying, at a first-order approximation, spontaneous ongoing activity and evoked response are two distinct processes, which can be registered both electrophysiologically and hemodynamically. Furthermore, sensory stimulation is known to induce robust enhancement in the high-frequency local field potential (LFP) signal, which correlates with the evoked BOLD response (Logothetis et al. 2001; Niessing et al. 2005). Inspired by these observations, we modulated brain activity by continuous unilateral whisker deflection at different frequencies, and performed epidural EEG recording and fMRI experiment. We reason that continuous whisker stimulation will not only induce high-frequency LFP oscillations, it will also entrain low-frequency (delta) oscillations, thus modulating brain activity across a wide spectral range. Our data show that changes in low-frequency EEG power (<5 Hz) synchrony induced similar changes in fMRI BOLD functional connectivity in bilateral whisker barrel cortex (WBC), and support the role of spontaneous fluctuations in low-frequency EEG signal underlying rsMRI.

## Materials and Methods

### Whisker Deflection Apparatus

In contrast to electrical stimulation of the rodent whisker pad, which is limited to individual electrical pulses, mechanical deflection of whiskers permits continuous sensory stimulation, and has been used in a number of fMRI studies (Yang et al. 1997; Lu et al. 2004). A computer-controlled whisker stimulator was customized, similar to the one used in a previous study (Lu et al. 2004). Briefly, a sinusoidal waveform was generated by a laptop computer, power-amplified, and used to drive a piezoelectric device. A small comb (1.5 cm in length, 1 cm in height, 12 teeth) was connected to the piezoelectric device through an actuator arm so that the amplitude, frequency, and duration of the backward/forward displacement of the comb could be prescribed. Stimulation parameters (waveform, frequency, amplitude) were calibrated using a Laser sensor device (ILD 1401, Micro-Optronic, Germany). The distance between the surface of the rat whisker pad and the comb was about 1 cm. As a result, only ~15 of the longest whiskers on the right side of the face were displaced. For fMRI experiments, an animal cradle and an aluminum table were customized to mount the stimulator onto the MRI platform (Fig. 1A). For epidural EEG recordings, the stimulator was mounted on the wall with the actuator arm passing into the Faraday recording cage to move the comb. This arrangement eliminated vibration artifacts from the whisker stimulator.

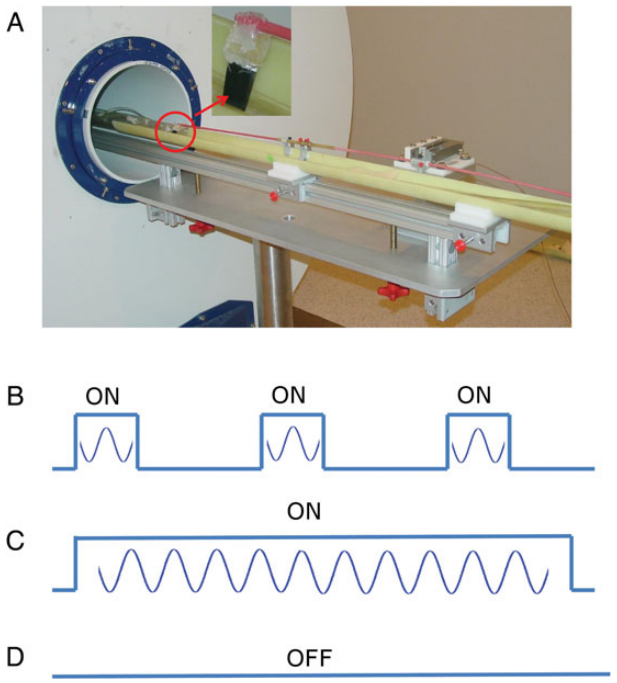


**Figure 1.** Experimental setup and schematic diagram of fMRI paradigms. (*A*) MRI-compatible whisker stimulator installed on the Bruker MRI platform. Red circle indicates the comb which was moved along the rostral–caudal direction by a rod actuated by the piezoelectric device. Three types of paradigm are employed in this study (*B–D*). (*B*) Block-design paradigm (20 s ON, 40 s OFF). This task was used to identify the whisker barrel cortex. (*C*) Continuous whisker stimulation (300 s ON; frequency: 2, 4, or 6 Hz; peak-to-peak amplitude of the sinusoidal wave form: 4 mm). (*D*) Resting condition during which no stimulation was applied (300 s OFF).

### Animal Preparation

Animal preparation was similar to a previous report (Lu et al. 2012). Briefly, a total of 19 Sprague-Dawley rats weighing (250–350 g) were used in this study. Animals were initially anesthetized with 3% isoflurane followed by intramuscular administration of the $\alpha_2$-agonist (dexmedetomidine, 0.015 mg/kg). A femoral artery was catheterized for measuring blood gases (model: GEM Premier 3000, Instrumentation Laboratory, MA, USA). Rats were then intubated and positioned into a customized cradle made out of G10 fiberglass, which has susceptibility close to air. An aluminum guide system was constructed to manually move the cradle in and out of the magnet (see Fig. 1). Animals were mechanically ventilated (model: SAR-830 ventilator, CWE, Inc., PA, USA) and respiration rate fixed at 60 bpm, while the tidal volume was carefully adjusted to maintain arterial blood gas levels. A small triple-bifurcate plastic tube was used to route expired air from the intubation tube to a gas analyzer (GEMINI Respiratory Monitor, CWE, Inc.), allowing for dynamically monitoring of tidal $CO_2$ and $O_2$ levels. Continuous intramuscular infusion of dexmedetomidine (0.015 mg/kg/h) was delivered using an infusion pump. Isoflurane concentration was gradually tapered to 0.5% in oxygen-enriched air, and was delivered via an artificial ventilator. A noninvasive pulse oximeter (Starr Life Sciences Corp., PA, USA) was connected to a hind paw to continuously monitor arterial oxygen saturation, which was maintained above 96% by adjusting the oxygen concentration in the gas mixture. Core body temperature was measured (TC-1000 temperature controller, CWE, Inc.) and maintained at 37.5 ± 0.3°C

using a water-circulating heating pump. A separate computer running WinDaq data acquisition software (DATAQ Instruments, OH, USA) was used to digitize the temperature, end-tidal $CO_2$ and $O_2$, cardiac and respiration signals, which were dynamically displayed on the operator's console and continuously monitored. All procedures were approved by the NIDA-IRP Animal Care and Use Committee.

## fMRI Data Acquisition and Analysis

fMRI experiments ($N = 9$) were carried out with a Bruker Biospin 9.4T scanner (Bruker Medizintechnik, Karlsruhe, Germany) equipped with an actively shielded gradient coil. A Bruker birdcage coil (inner diameter 72 mm) driven in linear mode was used for RF excitation. Since the Bruker surface receive-only coil interfered with the movement of the comb, a single-turn circular surface coil that accommodates the whisker stimulator was constructed for MR signal reception. This coil was made out of 13-gauge copper wire with an inner diameter of 1.8 cm. It featured an active decoupling circuit. Tuning and matching of the coil was performed for each animal with 2 rods extending to the back of the magnet. High-resolution $T_2$-weighted anatomical images were acquired using a rapid acquisition with relaxation enhancement (RARE) sequence. Scan parameters: TR = 2500 ms, effective TE = 40 ms, RARE factor = 8, field of view (FOV) = 3.5 × 3.5 $cm^2$, matrix size = 256 × 256, a total of 23 slices was acquired with a slice thickness of 1 mm. The decussation of the anterior commissure (–0.36 mm from bregma) served as the landmark to localize slices, which appeared dark in $T_2$-weighted saggital anatomical images and could be readily identified (see Supplementary Fig. 1). The center of WBC is about 2 mm posterior to bregma (Paxinos and Watson 2007). Functional images were acquired using a gradient echo echo-planar imaging (EPI) sequence. Scan parameters: FOV = 3.5 × 3.5 $cm^2$, matrix size = 64 × 64, TR/TE = 1000/15 ms, a total of 13 slices was acquired with a slice thickness of 1 mm. Data acquisition bandwidth was 250 kHz.

fMRI data were acquired 90 min after the initiation of dexmedetomidine administration since our previous study suggested that stable evoked BOLD responses began after this time point, presumably because animal physiology reached a stable steady-state condition (Lu et al. 2012). For each animal, activation of the WBC was first identified following whisker deflection, which was subsequently used as seed regions for rsMRI data analysis. Stimulation paradigm was a block design consisting of 20 s prestimulus baseline followed by 3 cycles of 20 s ON and 40 s OFF. During the ON period, whiskers were displaced sinusoidally at 6 Hz with the peak-to-peak amplitude of 4 mm; no stimulus was delivered during the OFF period. This was followed by continuous-task scans during which whiskers on the right side were continuously deflected at 2, 4, or 6 Hz in a pseudorandom order, interspersed with resting periods during which no whisker deflection was delivered. Each of these resting and continuous-task scans lasted for 5 min. Figure 1*B–D* illustrates the experimental paradigm. Due to technical limitations, we were not able to apply whisker stimulation with higher frequencies because it was found that the displacement of the comb at higher frequencies was not reliable in the current high-field small-bore MRI settings.

Geometric distortions in EPI images were corrected using the PLACE method (Xiang and Ye 2007). Raw EPI images in Supplementary Figure 2 illustrate data quality after geometric distortion correction. Images from individual animals were then co-registered onto a common 3D space aligned with a rat stereotaxic atlas using an approach previous described (Lu et al. 2010). Supplementary Figures 3 and 4 illustrate the quality of co-registration. Analyses were performed within the AFNI framework (Cox 1996). Specifically, for BOLD response to whisker stimulation using the block-design paradigm (Fig. 1*B*), individual time courses were first normalized to the prestimulus baseline. Data were then de-trended using second-order polynomials. Voxel-wise BOLD response waveforms were derived using the 3dDeconvolve function in AFNI. The amplitude of BOLD response in each voxel was calculated by computing the area under the curve of the BOLD waveform. Group activation maps were derived by voxel-wise Student's *t*-test against the null hypothesis and thresholded at $P < 0.005$ with a cluster size of 8. BOLD response curves in regions of interest (ROIs) were computed by averaging time courses in individual areas, which were then further averaged across animals.

rsMRI data (see Fig. 1*D*) were processed as follows: preprocessing steps included slice-timing correction, linear, and quadratic trend removal, spatial smoothing with a Gaussian kernel [full width at half maximum (FWHM) = 0.6 mm]. Data were low-pass filtered with a cutoff frequency of 0.1 Hz. Eleven voxel time courses from white matter (WM) were averaged to represent the WM signal, and fourteen voxels from lateral ventricle area were averaged to represent cerebral spinal flow signal. These 2 were considered nuisance signals related to physiological noise (mostly from respiration and cardiac pulsation), and were regressed out using the 3dDeconvolve function in AFNI. Eleven voxels in the center of the WBC activation maps (contralateral to whisker stimulation), along with 11 voxels mirrored on the contralateral WBC (ipsilateral to whisker stimulation) were chosen as ROIs. Time courses within each unilateral ROI were averaged to generate contra- or ipsilateral seed time courses, which served as reference functions to cross-correlate with voxel time courses of the entire brain. The resulting cross-correlation coefficients (CCs) were converted to *Z* scores via Fisher's *z*-transformation, which were then averaged within either the left or the right WBC to index the functional connectivity strength. The region of the WBC was defined based on the activation maps overlaid onto a rat digital atlas (Fig. 2).

EPI data acquired during continuous unilateral whisker stimulation at 2, 4, or 6 Hz (Fig. 1*C*) were analyzed in the same fashion as described above. Functional connectivity strength during the resting state and during each of the 3 continuous task states were subject to paired *t*-test. $P < 0.05$ was considered significant.

## Electrophysiological Recording and Data Analysis

Electrophysiological experiments followed a design parallel to the MRI experiments. Animals ($N = 10$) were placed in a Kopf stereotaxic device under isoflurane. The skull was exposed and 3 craniotomies (~2.5 mm diameter) were performed using a water-cooled drill. Two were centered at 2.4 mm posterior and 6 mm lateral to bregma over the left and right whisker barrel cortex and the third was centered at 7.0 mm posterior, 2.5 mm lateral to bregma over the right visual cortex. Semimicroelectrodes (SNEX-100X; Rhodes Medical Instruments, Inc., CA, USA) were stereotaxically placed on the intact dura at the center of each of the 3 locations while avoiding large blood vessels. Positions were adjusted slightly until robust evoked signals were recorded. Two stainless steel screws were positioned ~12 mm posterior and 3 mm lateral to bregma over the left and right cerebellar cortex, serving as reference and ground electrodes, respectively. Upon completion of surgery, isoflurane was reduced to 0.5% and continuous infusion of dexmeditomodine was initiated

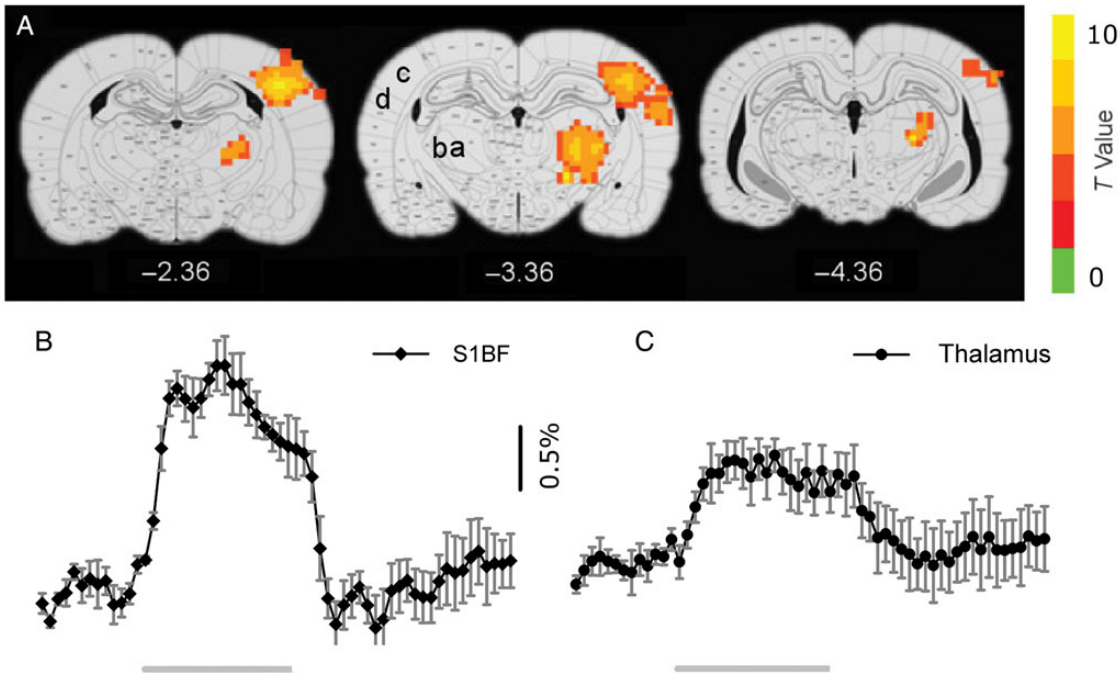


**Figure 2.** fMRI response to rat whisker barrel cortex stimulation. (*A*) Group statistical activation maps ($N = 9$) superimposed onto digital rat brain atlas. Activated areas include ventromedial and ventrolateral thalamic nuclei (VPM, VPL), primary whisker barrel cortex (S1BF), and secondary sensory cortex (S2). Numbers below figures are approximate coordinates relative to rat bregma. (*B* and *C*) Averaged BOLD responses in S1BF and thalamic nuclei (VPM and VPL) across animals ($N = 9$, mean ± SEM). The 2 gray lines below curves indicate the stimulus ON period, during which whiskers on the right side were deflected along the rostral–caudal direction. a and b: VPM, VPL; c: S1BF; d: S2.

following the same protocol as in the fMRI experiments. Rats were subsequently transferred into a Faraday cage. Epidural EEG signals were recorded using a multichannel data acquisition system (Plexon, Inc., TX, USA), and were amplified at a gain of 2000, bandpass-filtered at 0.3–2000 Hz, notch-filtered at 60 Hz, and digitally sampled at 4000 Hz. Each resting condition and continuous-task condition lasted for 5 min.

EEG data were analyzed in MATLAB (The MathWorks, Inc., Natick, MA, USA) and EEGLAB (Delorme and Makeig 2004). Data were downsampled to 256 Hz. Time–frequency analysis was performed using the complex Morlet wavelet:

$$\Psi_o(\eta) = \pi^{-1/4} \times \exp(i\omega_0 \times \eta) \times exp(-\eta^2/2), \quad (1)$$

where the parameter $\omega_0$ governs the relative time and frequency resolution, and was set to 6, which has been shown to provide a good trade-off between time and frequency localization (Torrence and Compo 1998; Grinsted et al. 2004). Note that $\Psi_o$ is normalized to unit energy at each scale, so that the wavelet transforms at each scale are directly comparable. Wavelet scales were set as fractional power of 2 with the smallest scale equal $2 \times \delta t$, here $\delta t$ is the data-sampling interval. There were a total of 57 scales which gave sufficient frequency resolution (Torrence and Compo 1998). At each wavelet scale, the wavelet power was derived by calculating the absolute values of the complex wave signal; power time course correlation between the 3 recording sites (bilateral WBC and the visual cortex) were then calculated and *z*-transformed. For display purpose, wavelet scales were converted to Fourier frequencies according to the method described by Torrence and Compo (1998). The EEG signal was also divided into 5 traditional frequency bands for power spectral analysis (delta: 1–4 Hz; theta: 5–8 Hz; alpha: 9–14 Hz; beta: 15–25 Hz; gamma: 26–50 Hz). Data are presented as mean ± standard deviation unless otherwise specified. Implementation of the wavelet transform was based on a library of MATLAB functions provided by Grinsted et al. (http://www.pol.ac.uk/home/research/waveletcoherence/).

Following wavelet transformation, time-domain EEG data were decomposed into the so-called "spectro-temporal" domain (Maris et al. 2007). For each recording electrode, there were 57 wavelet scales; each had its corresponding Fourier frequency. At each wavelet scale, there was a time course that reflected EEG power change as a function of time, which has the same temporal resolution as the raw EEG signal in the time domain. Wavelet-based time–frequency analysis thus offers a better compromise in spectral-temporal resolution than short-time Fourier-based time–frequency analysis. We calculated power correlations between the ipsi- and contralateral whisker barrel electrode pairs for each wavelet scale, resulting in a total of 57 correlation coefficients (CCs), which were transformed to *Z* scores. The same computations were performed between the visual and each of the whisker barrel electrode pairs.

In wavelet analysis, each wavelet scale has different window length, and thus different spectral resolution. Furthermore, the biological sources of the time courses at individual wavelet scales are not entirely independent. These factors together impose special challenges for statistical analysis. We applied a permutation-based, nonparametric statistical method according to the framework previously proposed (Lachaux et al. 2002; Maris and Oostenveld 2007; Maris et al. 2007) to compare the power correlation changes at the 3 stimulus conditions (2, 4, and 6 Hz) versus the resting condition, controlled for multiple comparisons, as detailed below:

Since the ipsilateral WBC-visual electrode pair had minimal response to whisker stimulation, we used data from this electrode pair to set statistical threshold (see Supplementary Fig. 5), controlling for false discovery rate (FDR) for the data acquired in

the ipsi- and contralateral whisker barrel electrode pair. Specifically, for a given wavelet scale, we pooled data from the 3 stimulus conditions together, and randomly assigned data from the stimulus ON and OFF conditions into 2 groups. With a total of 10 animals, we had a total of $2^{30}$ possible permutations. For the sake of efficiency, we performed 10 000 permutations. The difference in mean Z score between the 2 groups (noted as delta_Z) was calculated for each permutation, resulting in a histogram of delta_Z. A threshold of 5% was set from the histogram, reflecting 5% FDR, which was then applied to the data from the ipsi- and contralateral whisker barrel electrode pair. This procedure was repeated for each of the wavelet scales. Neighboring frequency bins that showed significant difference in delta_Z between the stimulus ON and OFF conditions were assigned to a spectral cluster. Cluster-level statistics controlling for multiple comparisons was then computed using the Monte Carlo approach (Maris et al. 2007). Specifically, data from the ipsi- and contralateral whisker barrel electrode pair with the stimulus ON and OFF conditions were randomly partitioned into 2 groups; delta_Z within the maximum spectra cluster was calculated. This process was repeated for a total of 10 000 times, resulting in a histogram of cluster statics, a threshold of $P < 0.05\%$ was considered significant.

## Results

### BOLD Response to Whisker Stimulation with the Block-Design Paradigm

Unilateral whisker stimulation induced robust BOLD responses in the contralateral WBC and thalamic nuclei. Figure 2A illustrates group activation maps displayed as overlay onto a digital atlas, allowing for accurate identification of the activated regions, which included ventroposterior medial and ventroposterior lateral thalamic nuclei (VPM, VPL), primary barrel field (S1BF), and secondary sensory cortex (S2). The activated regions correspond well to the expected major sensory processing pathway in rodents (Paxinos 1995). Figure 2B,C shows averaged BOLD responses ($N = 9$) in S1BF and thalamic nuclei (VPM, VPL), respectively.

### Comparison of Functional Connectivity During Rest versus Continuous-Task Condition

Functional connectivity was analyzed using the seed-based method (Biswal et al. 1995). Figure 3 shows raw connectivity maps from one animal. The seed was chosen on the side ipsilateral to whisker stimulation. The resting connectivity maps cover bilateral WBC and S2, consistent with previous report (Lu et al. 2012). However, with continuous unilateral whisker stimulation, the connectivity strength in the seed area (black arrow) was similar, but the connectivity strength contralateral to the seed region was reduced at 2 Hz, compared with 6 Hz (white arrows), and the connectivity strength at 6 Hz was similar to that during the resting condition. The same analysis was also performed with a seed on the side contralateral to whisker stimulation. Results were similar, although there were slight differences in areas of the connectivity maps, and thus are not shown here. Finally, we did not observe any anticorrelation patterns under these conditions.

We drew a WBC mask based on the activation maps and the digital atlas (Fig. 2A); a mirrored mask covering the homonymous WBC (ipsilateral to whisker stimulation) was also drawn. Connectivity strength within individual masks was averaged, and was compared between the resting and each task condition (2, 4, or 6 Hz). On the seed side, the connectivity strength was similar across the 4 conditions. This is expected, since the seed time course was used as the reference function for computing the CCs. But contralateral to the seed, in comparison to the resting condition, there was a reduction in connectivity strength at 2 Hz, but not at 4- or 6-Hz whisker stimulation (Fig. 4).

### Bilateral EEG Power Correlation Modulated by Unilateral Continuous Whisker Stimulation

Given the differential modulation of functional connectivity in bilateral WBC by unilateral whisker stimulation as shown above, we next explored its neurophysiological correlates, and performed epidural EEG recording in a separate group of identically prepared animals. Figure 5 illustrates 3 raw EEG traces downsampled to 256 Hz. It is apparent that the EEG signal was dominated by slow oscillations at 1–2 Hz during the stimulation OFF period. Unilateral whisker stimulation induced higher frequency components, while the amplitudes of low-frequency

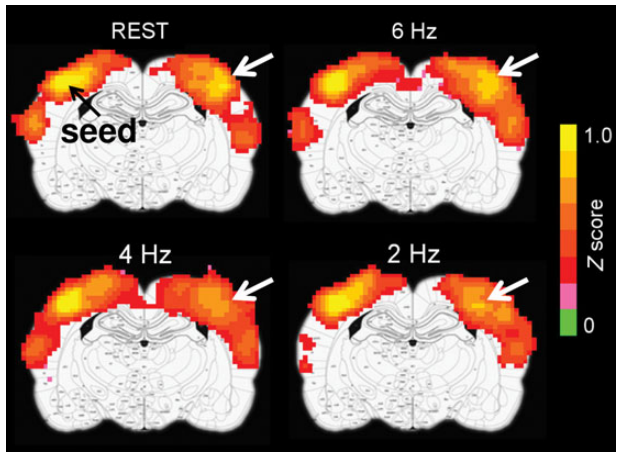


**Figure 3.** Raw functional connectivity maps during the resting condition and during continuous unilateral whisker stimulation (frequency: 2, 4, and 6 Hz). Data were from one representative animal. Seed voxels are on the left side; white arrows indicate differential functional connectivity strength on the contralateral barrel cortex.

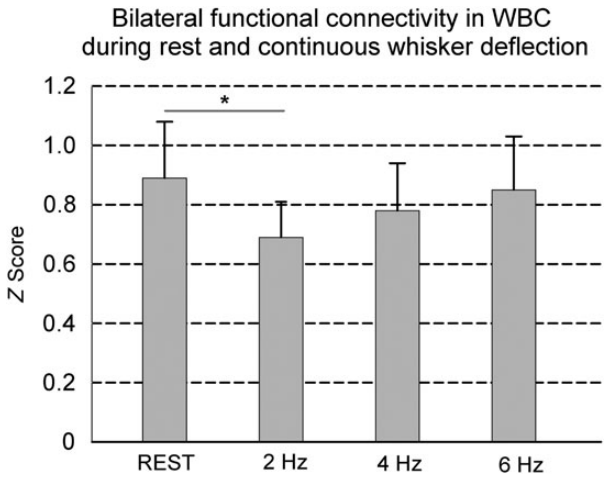


**Figure 4.** Comparison of functional connectivity during the rest and the 3 whisker deflection conditions (2, 4, and 6 Hz). Continuous unilateral whisker stimulation at 2 Hz, but not at 4 or 6 Hz, significantly reduces functional connectivity in bilateral whisker barrel cortex ($N = 9$; $^*P = 0.001$).

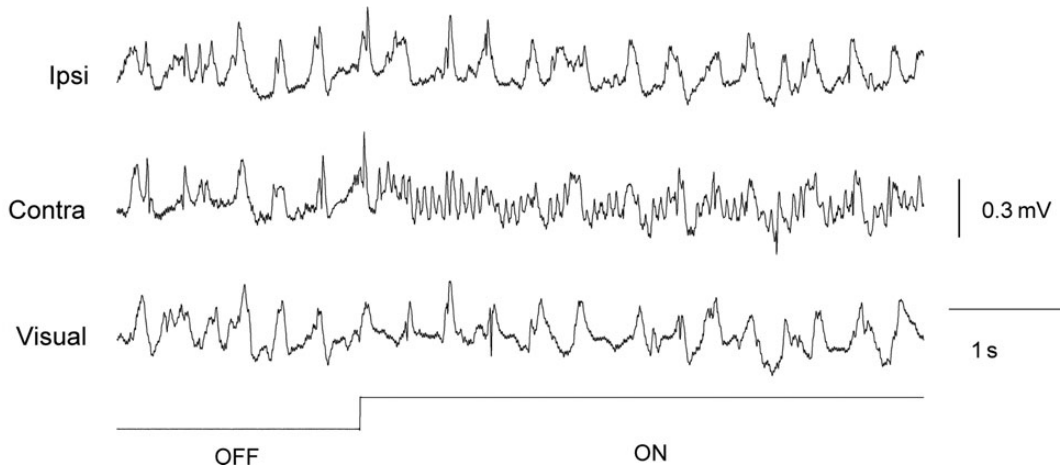


**Figure 5.** Raw epidural EEG traces from 3 recording sites (downsampled to 256 Hz). Unilateral whisker stimulation induces an enhancement in high-frequency component and a reduction of amplitude in the low-frequency component. Ipsi, barrel cortex ipsilateral to whisker deflection; Contra, barrel cortex contralateral to the whisker deflection; Visual, visual cortex. ON and OFF indicate periods during which the stimulator was turned on and off, respectively.

component were slightly suppressed (de-synchronization). This observation is similar to previous reports in mouse WBC (Crochet and Petersen 2006; Mohajerani et al. 2010). Quantitative analyses across animals ($N = 10$) revealed a 9.1 ± 4.3% reduction in power in the delta band, while increases in power were seen across all higher frequency bands: 18.8 ± 18.6% in theta, 57.4 ± 37.5% in alpha, 360.9 ± 190.2% in beta, and 170.3 ± 87.6% in gamma band.

We then computed power time courses using the wavelet analysis method. For each recording site, there were 57 time courses corresponding to 57 wavelet scales. For each wavelet scale, we calculated power CCs between individual recording electrodes. There were 57 CCs between 2 electrode pairs, which were then transformed to Z score for group comparison controlled for multiple comparisons using a nonparametric approach (Lachaux et al. 2002; Maris et al. 2007). The left panel in Figure 6 illustrates power correlations across 57 wavelet scales (each corresponds to one Fourier frequency) in the continuous-task condition (2, 4 or 6 Hz) versus the resting condition (during which no stimulation was applied). The right panel shows statistical results displayed in an exponential scale ($e^x$) for visual clarity. At the 6-Hz stimulus condition, significant changes in bilateral WBC power correlation were seen in the frequency bins of 6.5–33.8 Hz; At the 4-Hz stimulus condition, significant changes were seen in the frequency bins of 7.1–20.1 and 43.8–62 Hz; At the 2-Hz stimulus condition, significant changes were seen in the frequency bins of 7.1–21.9, 0.97–1.37, and 3.26–4.6 Hz. Thus, across all 3 continuous-task conditions, we observed significant changes in bilateral WBC power correlation at frequencies >5 Hz (indicated by gray shading). On the other hand, changes in power correlation in the low-frequency (<5 Hz) band were seen only at a stimulation frequency of 2 Hz, but not at 4- or 6-Hz stimulation condition.

## Discussion

In the present study, we found that low-frequency (<0.1 Hz) spontaneous BOLD fluctuations in bilateral WBC was modulated by unilateral continuous whisker stimulation at 2 Hz, but not at 4 or 6 Hz. Electrophysiologically, epidural EEG recording revealed that, in the high-frequency ranges (>5 Hz), power correlation in bilateral WBC was significantly modulated across all whisker stimulation conditions. However, only in the delta-frequency range was the power correlation significantly modulated at 2 Hz, but not at 4- or 6-Hz stimulation condition, paralleling the fMRI findings. EEG power correlation in other frequency ranges were similarly modulated irrespective of the stimulus conditions.

### Neural Correlate of the Resting-State fMRI Signal

Robust neurovascular coupling has been the corner stone of functional neuroimaging (Raichle 2001). Data accumulated over the past decades point to the tight correlation between the fMRI BOLD signal and LFPs, with the latter being a mass neural signal that captures a multitude of neural processes, including excitatory and inhibitory synaptic potentials, after-potentials and voltage-gated membrane oscillations, reflecting both the input of a given area as well as its local intracortical processing (Lauritzen and Gold 2003; Logothetis 2003). In the context of rsMRI, there have been substantial efforts to elucidate the neuronal basis of spontaneous BOLD fluctuations. Human EEG and MEG studies generally reported broad linkage between brain electrical activity and rsMRI signal (Mantini et al. 2007; Laufs 2008; de Pasquale et al. 2010; Hlinka et al. 2010). Several studies emphasize the role of alpha rhythm in the temporal dynamics of the resting BOLD signal (Goldman et al. 2002; Laufs et al. 2006; Chang et al. 2013). A number of studies reported that correlational activity in the high-frequency band (gamma band) underlies the rsMRI signal (Nir et al. 2008; Shmuel and Leopold 2008; Murayama et al. 2010). Given the nature of tight neurovascular coupling, it is conceivable that brain electrical activity at all frequency bands will have their hemodynamic signatures (Leopold et al. 2003; Schölvinck et al. 2010; Wang et al. 2012). The challenge, however, is to find the major electrophysiological driving force that underlies the rsMRI signal. Theoretically, if certain frequency bands of the LFP signal are identified as the major contributor to the rsMRI signal, then by modulating brain electrical activity within these bands, one should expect modulations in corresponding functional connectivity measured by rsMRI.

In the present study, we reasoned that if the high-frequency LFP signal underlies rsMRI, then by modulating brain electrical activity within these bands, we should expect modulations in corresponding fMRI functional connectivity. This supposition was not supported by our data: significant changes in power correlation were observed across all 3 tested stimulation conditions

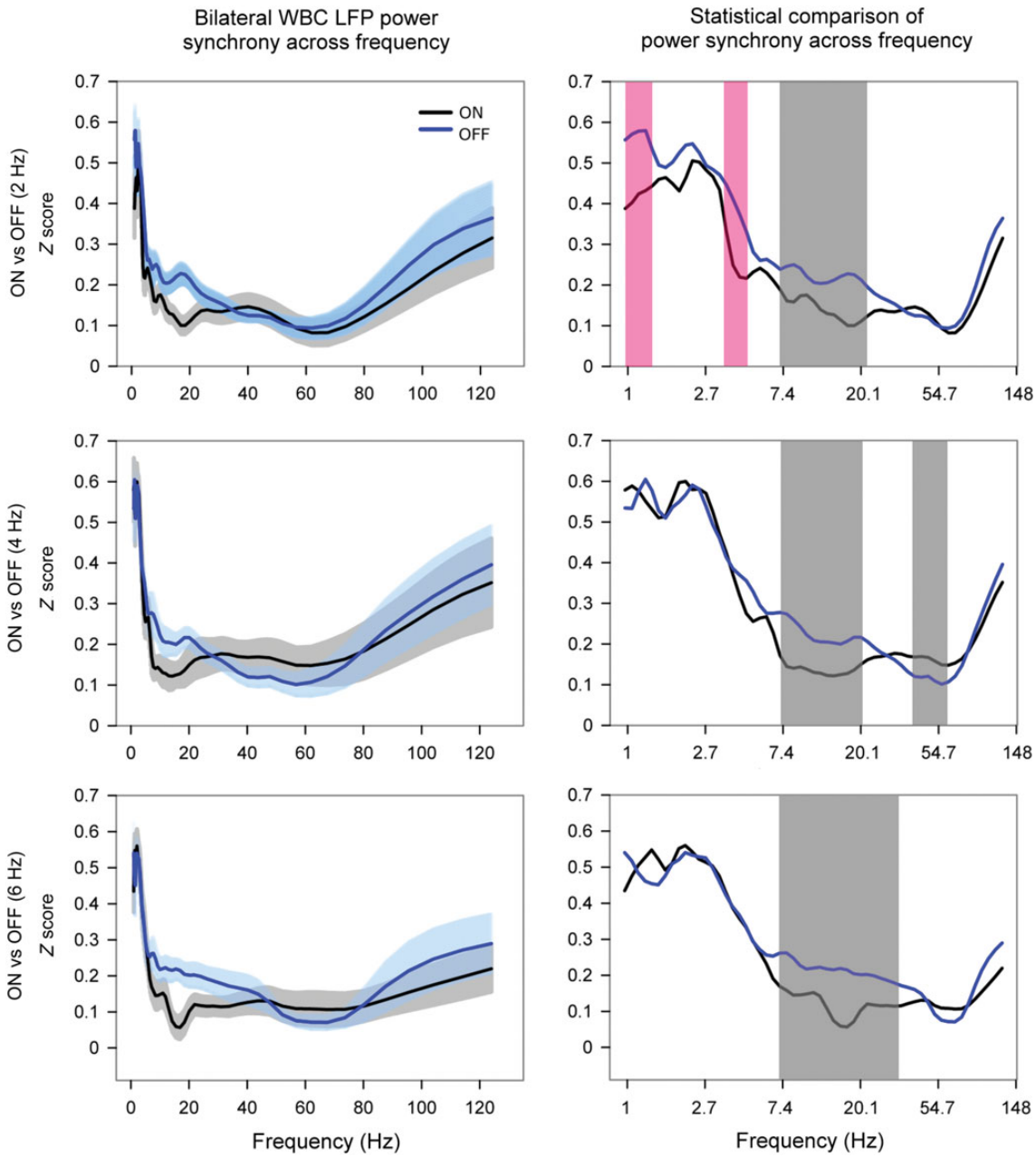


**Figure 6.** Comparison of power correlation during stimulus ON versus OFF period. Left panel: Plots of LFP power synchrony between bilateral whisker barrel cortices as a function of spectral frequency analyzed with the Morlet wavelet method. The correlation coefficients of the power time courses at each wavelet scale (Fourier frequency) were converted to Z score. Data are displayed as mean ± stand error. Note that unilateral whisker stimulation significantly reduced power correlations in low-frequency range (<5 Hz, pink shading) under the 2-Hz stimulus condition; power correlation at higher frequency ranges (>6 Hz, gray shading) was reduced across all 3 whisker stimulation conditions (2, 4, and 6 Hz). X-Axis is at exponential scale ($e^x$) for visual clarity.

(2, 4, and 6 Hz), but only at the 2-Hz stimulation condition did we observe significant changes in functional connectivity. On the other hand, when the whisker deflection induced power correlations in the delta band, we also observed changes in functional connectivity. In a recent optical imaging study using voltage-sensitive dye to measure membrane potentials and intrinsic signal to index hemodynamic response (Li et al. 2014), hemodynamic signal correlational maps were highly similar to those generated by slow cortical potentials (0.1–4 Hz), In contrast, neural activities measured at higher frequency bands appear to play only a minor role. These results are generally in line with previous reports using voltage-sensitive dye imaging (Mohajerani et al. 2010) and intrinsic optical imaging (White et al. 2011). Our results together with previous reports support the view that spontaneous activity in the delta band drives the rsMRI signal (Lu et al. 2007; He et al. 2008; Raichle 2011; Pan et al. 2013).

## Functional Roles of Delta Oscillations

Low-frequency oscillations, in particular, the delta oscillations, have been traditionally considered to index sleep stages (Steriade and Amzica 1998). Recent data demonstrate that such low-

frequency oscillations reflects rhythmic shift in the excitability of local neuronal ensembles. Indeed, hierarchical control of neuronal excitability by "cross-frequency phase–amplitude coupling" has been suggested (Lakatos et al. 2005), with the phase of delta oscillation modulating the amplitude of theta oscillation, and theta phase modulating gamma amplitude, leading to the proposition that gamma is the slave to, not the master of, lower frequency activity (Schroeder and Lakatos 2009). More recent evidence suggests that delta-band oscillations can function as an instrument of attentional selection (Lakatos et al. 2008). In that study, monkeys were trained to perform an intermodal selection task in which auditory and visual stimuli were delivered in a rhythmic, interdigitated stream. Although activity in the granular layer entrains to the input stream, as evidenced by amplitude modulation; delta oscillations in the supragranular layers were in opposite phase in the 2 attention conditions, suggesting a relationship between delta oscillation phase and neuronal excitability. Such "cross-frequency phase–amplitude coupling" was also apparent in rat striatal system, where cells fire only during the hypopolarized up-state (Goto and O'Donnell 2001). In another study involving simultaneous surface EEG, intracortical LFP, and multiunit activity (MUA) measurement (Whittingstall and Logothetis 2009), it has been shown that, in single trials, EEG power in the gamma band (30–100 Hz) and phase in delta band (2–4 Hz) are significant predictors of the MUA response. MUA response was strongest only when increases in EEG gamma power occurred during the negative-going phase of the delta wave. These data together suggest that cross-frequency phase–amplitude coupling may be a fundamental mechanism of brain operation.

Identifying the key role of delta oscillations in rsMRI signal could have important implications for the interpretation and application of spontaneous BOLD fluctuations and large scale brain network function. One notable, but somewhat "puzzling" feature of resting-state functional connectivity networks is their relatively widespread localization, not centering on specific fine structures as typically observed in evoked BOLD response. For example, the so-called default mode network (DMN) encompasses a number of association and limbic cortices, including medial prefrontal, anterior cingulate, posterior cingulate, hippocampal, and parahippocampal cortex (Raichle et al. 2001; Greicius et al. 2003). What binds these spatially disparate areas together? Studies with pharmacologically isolated networks and theoretical modeling suggest that gamma oscillations are generated by rhythmic synchronization of interneurons with excitatory drive from pyramidal cells (Fries et al. 2007). Such oscillations are typically confined to local networks. Making individual DMN structures fire together would require the excitability of local neurons to be in phase. We reason that low-frequency oscillations are well suited to do so through the mechanism of cross-frequency phase–amplitude coupling given that low-frequency oscillation reflects rhythmic shift in cell excitability (Lakatos et al. 2005). This idea is consistent with the proposition that gamma band oscillations serve as a "slave" to low-frequency activity (Schroeder and Lakatos 2009). Furthermore, unlike gamma synchronization, delta synchronization covers large areas (von Stein and Sarnthein 2000); this could also explain the relatively widespread localization of resting-state functional connectivity networks.

## Ongoing Spontaneous Activity Modulated by Tasks

The relationship of and interaction between ongoing spontaneous activity and task-induced brain activity has been a subject of great interest. Performance of a sustained attention-demanding working memory task attenuates correlational spontaneous activity in the DMN (Fransson 2006). A recent study reported that, using an N-back task, the functional connectivity within both the working memory network and the DMN was enhanced with increasing cognitive load (Newton et al. 2011). Another study comparing declarative versus nondeclarative memory-encoding tasks reported enhanced ongoing spontaneous activity in episodic memory-related circuitry (Xu et al. 2006). In the language system, functional connectivity was enhanced by continuously listening to narrative text (Hampson et al. 2002). In the sensory motor system, continuous bilateral finger tapping increases functional connectivity between primary and supplementary motor cortex at 1 Hz, but not at 2 or 4 Hz relative to resting state (Newton et al. 2007). Thus, the net effect of continuous task on spontaneous ongoing activity appears complex, depending on not only the types of task, but also brain system.

What neural mechanism could underlie such diverse effects? Our data suggest a possible explanation and prediction: for the rsMRI signal to be modulated, the low-frequency LFP band signal should be modulated. The direction of modulation (increase or decrease in functional connectivity) can be derived by low-frequency LFP or vice versa.

## Comparison with Previous Studies

Data from multiple laboratories support the notion that task-induced BOLD response correlates with broadband LFP signal. The study by Niessing et al. (2005) in the visual cortex of the anesthetized cat offers an example: low-frequency activity in the delta band showed a strong "negative" correlation with hemodynamic signal measured by intrinsic optical imaging; gamma band power, in particular the high gamma band, showed a strong "positive" correlation. A more recent study in the visual cortex of nonanesthetized monkeys (Magri et al. 2012) also confirmed that BOLD signal reliably followed gamma power changes; they further showed that relative power in alpha, beta, and gamma bands affected the amplitude and the latency of BOLD response. In the context of rsMRI, spontaneous fluctuations in gamma band power have been reported to correlate with rsMRI signal in monkeys and human (Nir et al. 2008; Shmuel and Leopold 2008; Murayama et al. 2010). Another study (Schölvinck et al. 2010) reported that the spontaneous fluctuations in LFP measured at rest from a single cortical site in monkeys exhibit widespread, positive correlations with fMRI signals over nearly the entire cerebral cortex. This correlation was especially consistent in a band of upper gamma-range frequencies (40–80 Hz), for which the hemodynamic signal lagged the neural signal by 6–8 s. A strong, positive correlation was also observed in a band of lower frequencies (2–15 Hz), with a lag close to zero. In rats anesthetized with isoflurane, broadband LFP power has been reported to correlate with rsMRI signal (Liu et al. 2011), with gamma activity being most tightly correlated with the local BOLD signal but delta power correlation being most predictive of functional connectivity as the depth of anesthesia changed (Pan et al. 2011). In another rat study involving callosotomy, in comparison to reduced functional connectivity in bilateral sensory cortex of the rat, reduction in broadband LFP power synchrony was observed with delta and gamma bands showing the greatest reduction (Magnuson et al. 2014).

Both our previous study (Lu et al. 2007) and our current data emphasize the role of low-frequency synchrony, particularly delta activity, underlying the rsMRI signal, which is to some extent, at variance with several previous reports. One technical

issue should be considered when comparing these studies: our electrophysiological data were acquired using semimicroelectrodes on the dura while others employed intracortical microelectrode recording. One advantage of our approach is that the epidural EEG signal likely reflects neuronal activity from the entire ROI (WBC), against which the BOLD signal is compared. In contrast, however, sensitivity to pick up high-frequency gamma activity is much lower with epidural recording. This technical limitation may have contributed to some of the differences mentioned above. Anesthesia regimes should also be taken into consideration (see below).

### Limitations and Technical Considerations

In general, the spatial and temporal scales of electrophysiological measures do not match that of fMRI. Depending on the recording site and the electrode properties, MUA has been estimated to represent the weighted sum of the extracellular action potentials from neurons within a sphere of 140–300 μm radius around the electrode; LFPs recorded with intracortical microelectrodes reflect a weighted average of synchronized dendrosomatic components of the synaptic signals from neural population within 0.5–3 mm of the electrode tip (Logothetis 2003). On the other hand, fMRI is generally measured on a spatial scale of millimeters (although high-field imaging could somewhat improve spatial resolution). Spatial smoothing and group averaging further reduces spatial resolution. Temporally, fMRI is measured on a level of seconds, while LFP signal covers a wide range of frequencies, from DC signal to fast changing gamma activity up to hundreds of Hertz. Such mismatches in spatial and temporal scales could intrinsically misguide comparison of the 2 types of signals. In this study, we measured WBC EEG signal epidurally, which presumably reflects the electrophysiological signal from the entire WBC (but likely also beyond WBC due to volume conduction), resulting in low sensitivity to high-frequency EEG components. fMRI signal was averaged across the entire WBC for comparison. This strategy has essentially abolished the functional connectivity information on a meso-scale of 100 μm. In this regard, experiments combining voltage-sensitive dye imaging with simultaneous intrinsic optical imaging offers certain advantages, since these 2 techniques have similar spatial resolution, and ambiguity due to volume conduction is entirely eliminated (see Lu and Stein (2014) for a more detailed discussion).

The methodological rationale of this study lies in unilateral modulation of WBC activity. However, bilateral barrel cortices are known to have strong callosal connections. Physiologically, complex neuroplasticity occurs in the ipsilateral cortex following unilateral peripheral nerve injury, as demonstrated by enhanced BOLD response and neuronal activity to ipsilateral electrical stimulation of the nerve (Pawela et al. 2008; Pelled et al. 2009). Simultaneous neurophysiology and fMRI study by Ogawa et al. (2000) also demonstrated complex interaction between bilateral sensory cortices. Thus, the interpretation of our data could have potentially oversimplified the complexity of brain processes.

In the present study, we employed a "reductionist" approach, and anesthetized the animals, which permitted differential manipulation of brain activity electrically and hemodynamically, as shown in Figures 2 and 5. A key question is whether the findings from the anesthetized preparation can be extrapolated to the conscious condition, and ultimately to humans. Clearly, the attentional, motivational and affective components involved in task performance in humans cannot be readily mimicked in the anesthetized preparation. Furthermore, anesthetics, such as isoflurane and dexmedetomidine, modulate multiple neurotransmitter systems at the cellular level (Brown et al. 2011), which in turn modulates both neuronal and hemodynamic responses to whisker stimulation. These factors together could limit the generalization of the findings. Further experiments are necessary to examine whether the same effect exists under different anesthetics or with different types of stimulation, and ultimately in human subjects. In the latter regard, Amann et al. (2009) employed a unilateral (right hand) finger tapping task, and found that functional connectivity between bilateral primary motor cortex was distinctively reduced with a self-paced tapping frequency of roughly 1 Hz, a finding corroborated by our animal data. Unfortunately, Amann et al. did not report how the functional connectivity would be modulated by finger tapping at higher frequencies (e.g., 6 Hz), presumably limited by task difficulty.

Due to multiple technical challenges, we performed electrophysiological recordings and fMRI experiments in 2 separate groups of animals. It would have been ideal to perform these 2 measurements simultaneously within the same animal. Nevertheless, we believe the methodology employed is theoretically sound since we modulated brain activity instead of simply comparing ongoing brain activity (which would otherwise require simultaneous recordings, since spontaneous ongoing activity is not likely to remain the same at 2 different time windows). This is true as long as the experimental conditions during the separate recordings remain the same. In reality, since one cannot be certain that conditions remained exactly the same across preparations, the interpretation of our findings is limited should systematic variations in experimental conditions have arisen despite our efforts to the contrary. To overcome this potential limitation, future studies should perform simultaneous electrophysiological and fMRI recordings in both this and other model systems to examine the proposed hypothesis.

In summary, this study aimed at determining which frequency band(s) in the LFP signal correlates with the rsMRI signal. We systematically modulated brain activity in WBC by unilateral mechanical whisker stimulation. Despite the fact that 4- and 6-Hz whisker movement significantly modulated LFP signal in high-frequency ranges, the functional connectivity between bilateral WBC was not modulated. On the other hand, whisker movement at 2-Hz reduced LFP power synchrony in both high- and low-frequency ranges, and reduced bilateral WBC functional connectivity. Our findings support the hypothesis that spontaneous fluctuations in low-frequency LFP band correlates with the rsMRI signal.

## Supplementary Material

Supplementary material can be found at: http://www.cercor.oxfordjournals.org/.

## Funding

This work was supported by the Intramural Research Program, National Institute on Drug Abuse, National Institute of Health. H.L. benefited from discussions with Dr Asaf Keller of University of Maryland about EEG recording in the whisker barrel cortex.

## Notes

We thank Drs R. W. Cox and Z. S. Saad of NIMH and Dr T. J. Ross at NIDA for advice on statistical analysis, Drs A. C. Silva and H. Merkle at NINDS for building the surface coil. *Conflict of Interest:* None declared.

## References


Amann M, Hirsch JG, Gass A. 2009. A serial functional connectivity MRI study in healthy individuals assessing the variability of connectivity measures: reduced interhemispheric connectivity in the motor network during continuous performance. Magn Reson Imaging. 27:1347–1359.

Anand A, Mathews VP, Bukhari L, Yang W, Shirley JA, Jeffrey L, Lowe MJ. 2003. Functional connectivity within the mood regulating circuit in major depression—an fMRI study. Biol Psychiatry. 53:95S–96S.

Arieli A, Shoham D, Hildesheim R, Grinvald A. 1995. Coherent spatiotemporal patterns of ongoing activity revealed by real-time optical imaging coupled with single-unit recording in the cat visual cortex. J Neurophysiol. 73:2072–2093.

Arieli A, Sterkin A, Grinvald A, Aertsen A. 1996. Dynamics of ongoing activity: explanation of the large variability in evoked cortical responses. Science 273:1868–1871.

Biswal B, Yetkin FZ, Haughton VM, Hyde JS. 1995. Functional connectivity in the motor cortex of resting human brain using echo-planar MRI. Magn Reson Med. 34:537–541.

Brown EN, Purdon PL, Van Dort CJ. 2011. General anesthesia and altered states of arousal: a systems neuroscience analysis. In: Hyman SE, Jessell TM, Shatz CJ, Stevens CF, Zoghbi HY, editors. Annual review of neuroscience, Vol 34. p. 601–628.

Buzsaki G, Buhl DL, Harris KD, Csicsvari J, Czeh B, Morozov A. 2003. Hippocampal network patterns of activity in the mouse. Neuroscience. 116:201–211.

Buzsaki G, Draguhn A. 2004. Neuronal oscillations in cortical networks. Science 304:1926–1929.

Chang C, Liu ZM, Chen MC, Liu X, Duyn JH. 2013. EEG correlates of time-varying BOLD functional connectivity. Neuroimage. 72:227–236.

Chrobak JJ, Buzsaki G. 1998. Gamma oscillations in the entorhinal cortex of the freely behaving rat. J Neurosci. 18:388–398.

Cox R. 1996. AFNI: software for analysis and visualization of functional magnetic resonance neuroimages. Comput Biomed Res. 29:162–173.

Crochet S, Petersen CC. 2006. Correlating whisker behavior with membrane potential in barrel cortex of awake mice. Nat Neurosci. 9:608–610.

de Pasquale F, Della Penna S, Snyder AZ, Lewis C, Mantini D, Marzetti L, Belardinelli P, Ciancetta L, Pizzella V, Romani GL, et al. 2010. Temporal dynamics of spontaneous MEG activity in brain networks. Proc Natl Acad Sci USA. 107:6040–6045.

Delorme A, Makeig S. 2004. EEGLAB: an open source toolbox for analysis of single-trial EEG dynamics including independent component analysis. J Neurosci Methods. 134:9–21.

Engel AK, Fries P, König P, Brecht M, Singer W. 1999. Temporal binding, binocular rivalry, and consciousness. Conscious Cogn. 8:128–151.

Fox MD, Snyder AZ, Zacks JM, Raichle ME. 2006. Coherent spontaneous activity accounts for trial-to-trial variability in human evoked brain responses. Nat Neurosci. 9:23–25.

Fransson P. 2006. How default is the default mode of brain function? Further evidence from intrinsic BOLD signal fluctuations. Neuropsychologia. 44:2836–2845.

Fries P, Nikolic D, Singer W. 2007. The gamma cycle. Trends Neurosci. 30:309–316.

Goldman RI, Stern JM, Engel J, Cohen MS. 2002. Simultaneous EEG and fMRI of the alpha rhythm. Neuroreport. 13:2487–2492.

Goto Y, O'Donnell P. 2001. Synchronous activity in the hippocampus and nucleus accumbens in vivo. J Neurosci. 21:RC131.

Greicius M. 2008. Resting-state functional connectivity in neuropsychiatric disorders. Curr Opin Neurol. 21:424–430.

Greicius M, Krasnow B, Reiss A, Menon V. 2003. Functional connectivity in the resting brain: a network analysis of the default mode hypothesis. Proc Natl Acad Sci USA. 100:253–258.

Greicius MD, Flores BH, Menon V, Glover GH, Solvason HB, Kenna H, Reiss AL, Schatzberg AF. 2007. Resting-state functional connectivity in major depression: abnormally increased contributions from subgenual cingulate cortex and thalamus. Biol Psychiatry. 62:429–437.

Greicius MD, Srivastava G, Reiss AL, Menon V. 2004. Default-mode network activity distinguishes Alzheimer's disease from healthy aging: evidence from functional MRI. Proc Natl Acad Sci USA. 101:4637–4642.

Grinsted A, Moore JC, Jevrejeva S. 2004. Application of the cross wavelet transform and wavelet coherence to geophysical time series. Nonlin Processes Geophys. 11:561–566.

Gu H, Salmeron BJ, Ross TJ, Geng X, Zhan W, Stein EA, Yang Y. 2010. Mesocorticolimbic circuits are impaired in chronic cocaine users as demonstrated by resting-state functional connectivity. Neuroimage. 53:593–601.

Hampson M, Peterson BS, Skudlarski P, Gatenby JC, Gore JC. 2002. Detection of functional connectivity using temporal correlations in MR images. Hum Brain Mapp. 15:247–262.

He BJ, Snyder AZ, Zempel JM, Smyth MD, Raichle ME. 2008. Electrophysiological correlates of the brain's intrinsic large-scale functional architecture. Proc Natl Acad Sci USA. 105: 16039–16044.

Hlinka J, Alexakis C, Diukova A, Liddle PF, Auer DP. 2010. Slow EEG pattern predicts reduced intrinsic functional connectivity in the default mode network: an inter-subject analysis. Neuroimage. 53:239–246.

Hong LE, Gu H, Yang Y, Ross TJ, Salmeron BJ, Buchholz B, Thaker GK, Stein EA. 2009. Association of nicotine addiction and nicotine's actions with separate cingulate cortex functional circuits. Arch Gen Psychiatry. 66:431–441.

Jensen O, Kaiser J, Lachaux JP. 2007. Human gamma-frequency oscillations associated with attention and memory. Trends Neurosci. 30:317–324.

Lachaux JP, Lutz A, Rudrauf D, Cosmelli D, Le van Quyen M, Martinerie J, Varela F. 2002. Estimating the time-course of coherence between single-trial brain signals: an introduction to wavelet coherence. Neurophysiol Clin. 32:157–174.

Lakatos P, Karmos G, Mehta AD, Ulbert I, Schroeder CE. 2008. Entrainment of neuronal oscillations as a mechanism of attentional selection. Science 320:110–113.

Lakatos P, Shah AS, Knuth KH, Ulbert I, Karmos G, Schroeder CE. 2005. An oscillatory hierarchy controlling neuronal excitability and stimulus processing in the auditory cortex. J Neurophysiol. 94:1904–1911.

Laufs H. 2008. Endogenous brain oscillations and related networks detected by surface EEG-combined fMRI. Hum Brain Mapp. 29:762–769.

Laufs H, Holt JL, Elfont R, Krams M, Paul JS, Krakow K, Kleinschmidt A. 2006. Where the BOLD signal goes when alpha EEG leaves. Neuroimage. 31:1408–1418.

Lauritzen M, Gold L. 2003. Brain function and neurophysiological correlates of signals used in functional neuroimaging. J Neurosci. 23:3972–3980.

Leopold DA, Maier A. 2012. Ongoing physiological processes in the cerebral cortex. Neuroimage. 62:2190–2200.

Leopold DA, Murayama Y, Logothetis NK. 2003. Very slow activity fluctuations in monkey visual cortex: implications for functional brain imaging. Cereb Cortex. 13:422–433.

Li B, Liu R, Huang Q, Lu J, Luo Q, Li P. 2014. Coherent slow cortical potentials reveal a superior localization of resting-state functional connectivity using voltage-sensitive dye imaging. Neuroimage. 91:7.

Li SJ, Li Z, Wu G, Zhang MJ, Franczak M, Antuono PG. 2002. Alzheimer disease: evaluation of a functional MR imaging index as a marker. Radiology. 225:253–259.

Liu X, Zhu XH, Zhang Y, Chen W. 2011. Neural origin of spontaneous hemodynamic fluctuations in rats under burst-suppression anesthesia condition. Cereb Cortex. 21:374–384.

Logothetis NK. 2003. The underpinnings of the BOLD functional magnetic resonance imaging signal. J Neurosci. 23:3963–3971.

Logothetis NK, Pauls J, Augath M, Trinath T, Oeltermann A. 2001. Neurophysiological investigation of the basis of the fMRI signal. Nature. 412:150–157.

Lu H, Patel S, Luo F, Li SJ, Hillard CJ, Ward BD, Hyde JS. 2004. Spatial correlations of laminar BOLD and CBV responses to rat whisker stimulation with neuronal activity localized by Fos expression. Magn Reson Med. 52:1060–1068.

Lu H, Scholl C, Zuo Y, Demny S, Rea W, Stein E, Yang Y. 2010. Registering and analyzing rat fMRI data in the stereotaxic framework by exploiting intrinsic anatomical features. Magn Reson Imaging. 28:146–152.

Lu H, Stein EA. 2014. Resting state functional connectivity: its physiological basis and application in neuropharmacology. Neuropharmacology. 84:79–89.

Lu H, Zou Q, Gu H, Raichle ME, Stein EA, Yang Y. 2012. Rat brains also have a default mode network. Proc Natl Acad Sci USA. 109:3979–3984.

Lu H, Zuo Y, Gu H, Waltz JA, Zhan W, Scholl CA, Rea W, Yang Y, Stein EA. 2007. Synchronized delta oscillations correlate with the resting-state functional MRI signal. Proc Natl Acad Sci USA. 104:18265–18269.

Lustig C, Snyder AZ, Bhakta M, O'Brien KC, McAvoy M, Raichle ME, Morris JC, Buckner RL. 2003. Functional deactivations: change with age and dementia of the Alzheimer type. Proc Natl Acad Sci USA. 100:14504–14509.

Magnuson ME, Thompson GJ, Pan WJ, Keilholz SD. 2014. Effects of severing the corpus callosum on electrical and BOLD functional connectivity and spontaneous dynamic activity in the rat brain. Brain Connect. 4:15–29.

Magri C, Schridde U, Murayama Y, Panzeri S, Logothetis NK. 2012. The amplitude and timing of the BOLD signal reflects the relationship between local field potential power at different frequencies. J Neurosci. 32:1395–1407.

Mantini D, Perrucci MG, Del Gratta C, Romani GL, Corbetta M. 2007. Electrophysiological signatures of resting state networks in the human brain. Proc Natl Acad Sci USA. 104: 13170–13175.

Maris E, Oostenveld R. 2007. Nonparametric statistical testing of EEG- and MEG-data. J Neurosci Methods. 164:177–190.

Maris E, Schoffelen JM, Fries P. 2007. Nonparametric statistical testing of coherence differences. J Neurosci Methods. 163:161–175.

Mohajerani MH, McVea DA, Fingas M, Murphy TH. 2010. Mirrored bilateral slow-wave cortical activity within local circuits revealed by fast bihemispheric voltage-sensitive dye imaging in anesthetized and awake mice. J Neurosci. 30:3745–3751.

Murayama Y, Biessmann F, Meinecke FC, Müller KR, Augath M, Oeltermann A, Logothetis NK. 2010. Relationship between neural and hemodynamic signals during spontaneous activity studied with temporal kernel CCA. Magn Reson Imaging. 28:1095–1103.

Newton AT, Morgan VL, Gore JC. 2007. Task demand modulation of steady-state functional connectivity to primary motor cortex. Hum Brain Mapp. 28:663–672.

Newton AT, Morgan VL, Rogers BP, Gore JC. 2011. Modulation of steady state functional connectivity in the default mode and working memory networks by cognitive load. Hum Brain Mapp. 32:1649–1659.

Niessing J, Ebisch B, Schmidt KE, Niessing M, Singer W, Galuske RAW. 2005. Hemodynamic signals correlate tightly with synchronized gamma oscillations. Science. 309:948–951.

Nir Y, Mukamel R, Dinstein I, Privman E, Harel M, Fisch L, Gelbard-Sagiv H, Kipervasser S, Andelman F, Neufeld MY, et al. 2008. Interhemispheric correlations of slow spontaneous neuronal fluctuations revealed in human sensory cortex. Nat Neurosci. 11:1100–1108.

Ogawa S, Lee TM, Stepnoski R, Chen W, Zhu XH, Ugurbil K. 2000. An approach to probe some neural systems interaction by functional MRI at neural time scale down to milliseconds. Proc Natl Acad Sci USA. 97:11026–11031.

Pan WJ, Thompson G, Magnuson M, Majeed W, Jaeger D, Keilholz S. 2011. Broadband local field potentials correlate with spontaneous fluctuations in functional magnetic resonance imaging signals in the rat somatosensory cortex under isoflurane anesthesia. Brain Connect. 1:119–131.

Pan WJ, Thompson GJ, Magnuson ME, Jaeger D, Keilholz S. 2013. Infraslow LFP correlates to resting-state fMRI BOLD signals. Neuroimage. 74:288–297.

Pawela CP, Biswal BB, Cho YR, Kao DS, Li R, Jones SR, Schulte ML, Matloub HS, Hudetz AG, Hyde JS. 2008. Resting-state functional connectivity of the rat brain. Magn Reson Med. 59: 1021–1029.

Paxinos G, Watson C. 2007. The rat brain in stereotaxic coordinates. 6th ed. Amsterdam: Elsevier, Inc.

Paxinos GT. 1995. Rat nervous system. 2nd ed. London: Academic Press, Inc.

Pelled G, Bergstrom DA, Tierney PL, Conroy RS, Chuang KH, Yu D, Leopold DA, Walters JR, Koretsky AP. 2009. Ipsilateral cortical fMRI responses after peripheral nerve damage in rats reflect increased interneuron activity. Proc Natl Acad Sci USA. 106:14114–14119.

Raichle M, MacLeod A, Snyder A, Powers W, Gusnard D, Shulman G. 2001. A default mode of brain function. Proc Natl Acad Sci USA. 98:676–682.

Raichle ME. 2001. Cognitive neuroscience—bold insights. Nature. 412:128–130.

Raichle ME. 2011. The restless brain. Brain Connect. 1:3–12.

Schroeder CE, Lakatos P. 2009. The gamma oscillation: master or slave? Brain Topogr. 22:24–26.

Schroeder CE, Lakatos P. 2012. The signs of silence. Neuron. 74:770–772.

Schölvinck ML, Maier A, Ye FQ, Duyn JH, Leopold DA. 2010. Neural basis of global resting-state fMRI activity. Proc Natl Acad Sci USA. 107:10238–10243.

Shmuel A, Leopold DA. 2008. Neuronal correlates of spontaneous fluctuations in fMRI signals in monkey visual cortex: implications for functional connectivity at rest. Hum Brain Mapp. 29:751–761.

Steriade M, Amzica F. 1998. Sleep oscillation, rhythmic K-complexes, and their paroxysmal developments. J Sleep Res. 7:30–35.

Tomasi D, Volkow ND, Wang R, Carrillo JH, Maloney T, Alia-Klein N, Woicik PA, Telang F, Goldstein RZ. 2010. Disrupted functional connectivity with dopaminergic midbrain in cocaine abusers. PLoS One. 5:e10815.

Torrence C, Compo GP. 1998. A practical guide to wavelet analysis. Bull Am Meteorol Soc. 79:61–78.

von Stein A, Sarnthein J. 2000. Different frequencies for different scales of cortical integration: from local gamma to long range alpha/theta synchronization. Int J Psychophysiol. 38: 301–313.

Wang L, Saalmann YB, Pinsk MA, Arcaro MJ, Kastner S. 2012. Electrophysiological low-frequency coherence and cross-frequency coupling contribute to BOLD connectivity. Neuron. 76:1010–1020.

White BR, Bauer AQ, Snyder AZ, Schlaggar BL, Lee JM, Culver JP. 2011. Imaging of functional connectivity in the mouse brain. PLoS One. 6:e16322.

Whittingstall K, Logothetis NK. 2009. Frequency-band coupling in surface EEG reflects spiking activity in monkey visual cortex. Neuron. 64:281–289.

Xiang Q, Ye F. 2007. Correction for geometric distortion and N/2 ghosting in EPI by phase labeling for additional coordinate encoding (PLACE). Magn Reson Med. 57:731–741.

Xu GF, Xu Y, Wu GH, Antuono PG, Hammeke TA, Li SJ. 2006. Task-modulation of functional synchrony between spontaneous low-frequency oscillations in the human brain detected by fMRI. Magn Reson Med. 56:41–50.

Yang XJ, Hyder F, Shulman RG. 1997. Functional MRI BOLD signal coincides with electrical activity in the rat whisker barrels. Magn Reson Med. 38:874–877.